Energy-Based Design Optimization of a Miniature Wave-Like Robot inside Curved Compliant Tubes

Rotem Katz, Dan Shachaf and David Zarrouk

Abstract — This paper analyzes the crawling locomotion of a wave-like robot in curved tubes. We use an energy-based approach to determine the optimal crawling orientation of the robot that minimizes the surface energy while advancing. The results showed that the robot rotated its body along the roll direction so that the wave motion would be in the same plane as the curvature plane of the tube. The incorporation of a passive bending joint along the plane of the wave motion decreased the surface energy and enhanced the robot's ability to advance in even tighter curves. Given these findings we designed and manufactured two new robots with either one or two passive bending joints. We molded custom flexible surfaces and tubes and experimentally tested our robots in them. These validating experiments indicated that the bending joints substantially improved the robots' ability to traverse curved tubes (see video).

I. INTRODUCTION

In the past few decades, the field of medical robotics has evolved immensely. The need to devise new methods of treatment and diagnosis, along with progress in technology, has led to advances in the use of robots in complex medical procedures. These robots can range in size and carry out tasks that exceed human capabilities. Gastro-intestinal diagnoses, in particular, have evolved tremendously since the invention of capsule endoscopy [1]. Recent works have dealt with the characterization of the bowel, primarily in terms of its size and frictional traits [2]-[5]. Other studies have developed new mechanisms to enable robots to explore the bowel more comprehensively. Most of these robots take a minimalistic design approach, using novel methods for actuation and steering to keep the robots miniaturized. Many of these mechanisms are bio-inspired, in the sense that they imitate the motion of earthworms [6]-[10] that expand and contract segments of their bodies, and inchworms [11]-[16] that create a push-pull mechanism using two different contact points, or mimic the motion of snakes [17]-[20]. Although most of these mechanisms are based on multiple mechanical rotational motors to generate motion, others have used shape memory alloys (SMA) [21]-[22], magnetic propulsion [23], legged propulsion [24] and motor controlled cables [25]-[26] to produce different types of motion in a single actuated device.

In previous works, we presented the Single Actuated Wave robot (SAW) that produces undulating locomotion with a single motor [27] and a newer variant incorporating two waves attached to each other using an actuated U joint. This design had a total of four motors [28].

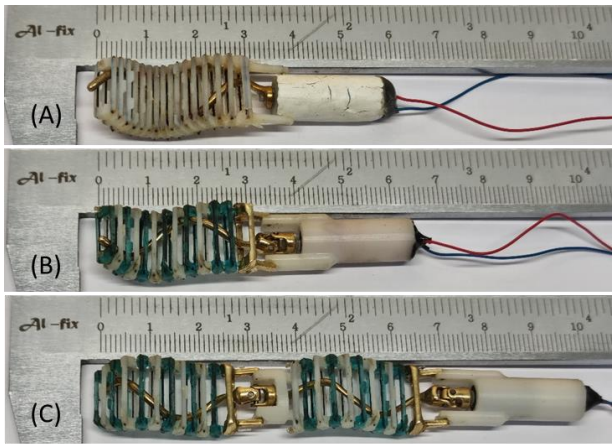

Figure 1. Three miniature versions of the SAW Robot. (A) Previously designed simple SAW measuring 57 mm in length and weighing 4.6 g. (B) The newly designed SAW with a bending joint 63 mm in length and weighing 5.8 g. (C) The newly designed SAW with two bending joints measuring 98 mm in length and weighing 8.7 g.

We also developed a miniature version of the robot (Figure 1A) that can advance in a variety of environments such as tough planar surfaces and compliant surfaces and tubes [29]-[30] and analyzed its locomotion but the analysis was limited to straight tubes. This model (with no joint) successfully advanced in pig intestines without causing any visible damage.

This paper examines the crawling locomotion of the SAW robot in curved flexible environments. We use an energy based analysis to improve the design. Given that the energy is related to the deformations of the tube and power consumption of the robot, minimizing the energy will help reduce the deformations and allow the robot to advance more smoothly in the pipes. Based on our results, we investigate the influence of adding one or two passive bending joints (in contrast to [28] where the joints are fully actuated) between the motor house to the wave and between one section of the wave to another (Figure 1, B and C respectively). Section II describes the design of these two robots. Section III, presents an energy-based analysis of the robot's motion in a planar environment between two compliant walls and determine the orientation which leads to the lowest surface energy. In Section IV, we present several experiments to test the robots. First, we validate our analysis by testing the robot's motion between two walls at different coefficients of friction (COF) and curvatures. Then, we test the robots in 2D and 3D tubes.

* Department of Mechanical Engineering, Ben Gurion University of the Negev, Israel (rotek@post.bgu.ac.il, shachafd@post.bgu.ac.il, zadavid@bgu.ac.il).

Finally, to evaluate the influence of the joints on locomotion, we compare the performance of the designs with no joints, one joint or two joints for traversability, speed and energy consumption.

II. Robot Design

This section overviews the robot's structure, the design process considerations and the modification upgrades that were made relative to the previous model [29]. The design takes multiple insights regarding the addition of an angular passive joint based on the analytical models presented in Section III.

A. Single-Wave Robot with a Single Bending Joint

The single-wave robot measures 63 mm in length, 15 mm in width and weighs 5.8 g. It is composed of three subassemblies. The first is the head, which provides a solid base for the links and houses a 6 mm DC motor that rotates the helix. The motor produces 10 mNm of torque at 37 RPM at maximum power which generates a wave speed of ($V_w = f \cdot L_w$) 22.8 mm/s where V_w is the wave speed, f is the rotation frequency and L_w = 37 mm is the wave length. The second subassembly is the rotating helix fitted with an in-house designed wax cast brass U-joint that permits the wave to bend relative to the motor housing by an angle $\beta \in [-60^o, 60^o]$; see Figure 2. This ability to bend gives the robot more flexibility when traversing curved tubes and pipes. Note that adding a second DOF of bending to the same joint was shown to cause the motor to spin around itself, therefore the concept was discarded. The last subassembly is a group of 15 links which form the wave and translate the rotation of the helix into a two-dimensional sinusoidal advancing wave that enables the robot to crawl. The links are attached to each other with nylon wire.

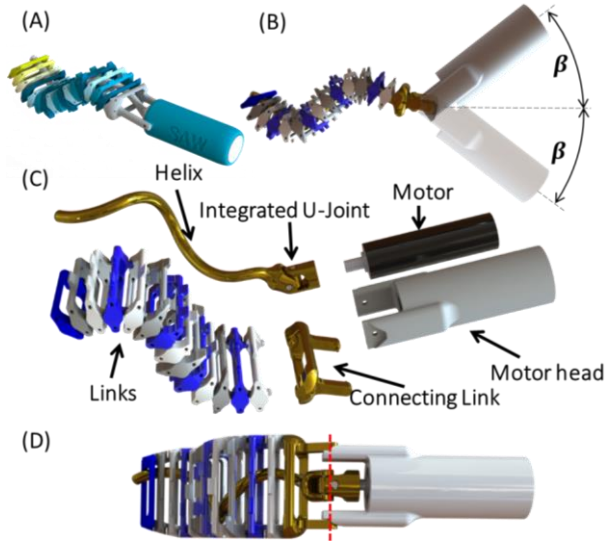

Figure 2. (A) The previous simple SAW design (without a passive bending joint). (B) The new design with a bending joint. The tail can bend relative to the head by $\pm\beta$. (C) An exploded view of the novel design which is comprised of a motor housing, a motor, a helix with an integrated U-joint, a connecting link, and a set of 15 links forming the tail. (D) The head design in which the axes of rotation of the connecting link and the U joint of the helix are co-linear, ensures smooth wave motion while preventing unwanted fluctuations.

The U-joint is integrated into the helix to provide a passive degree of freedom (DOF) between the motor housing (head) and the wave, thus giving the robot more flexibility when travelling through curved tubes. To ensure smooth rotational motion when $\beta \neq 0$, the axis of the connecting link crosses the center of the U-joint (Figure 2, D). This reduces the friction between parts, which thus channels more energy to the robot's forward motion while preventing jamming and increased fluctuations.

B. Double-Wave Robot with two Bending Joints

We also developed a double-wave robot built with the same subassemblies as the single wave but with an extra bending joint between the two waves. The double wave robot measures 98 mm in length, has a maximum width of 15 mm and weighs 8.7 g.

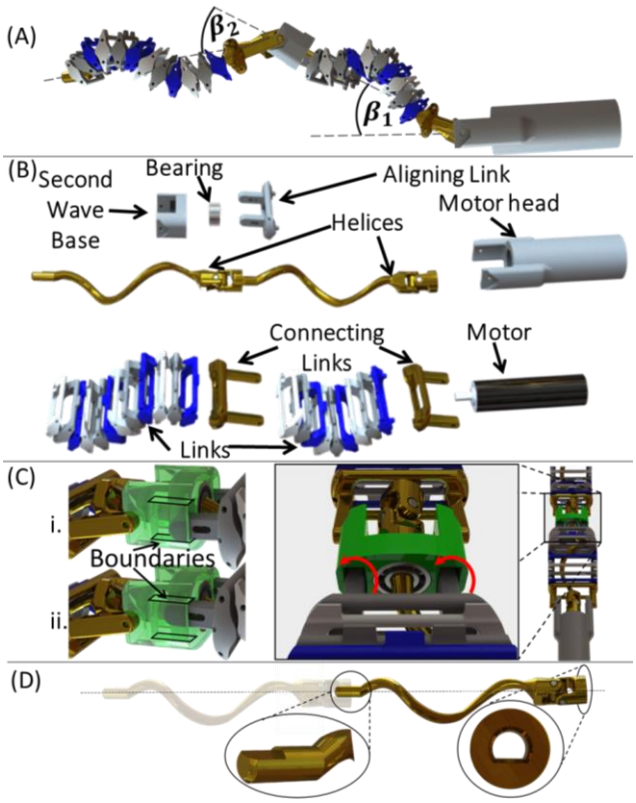

Figure 3. (A) The robot design with two waves, where the bend of the first wave relative to the motor housing is denoted by β_1 and the bend of the second wave relative to the first is denoted by β_2. Each joint can bend by up to 60 degrees. (B) An exploded view of the two- wave design comprised of a motor housing, a motor, two helices with an integrated U-joint each, two connecting links, two sets of links forming the tail and a base and an aligning link to connect the two waves. (C) Left – the position of the aligning link is bounded by two horizontal planes to be able to move between them freely while the wave is advancing (as depicted in i. and ii). Center and Right– slots in the second wave base enable up-down or forward-backward motion but prevent relative rotation between the base and aligning link. (D) Concatenation of two helices. The helices are designed so that multiple helices can be added when required.

In order to maintain the simplicity of the helix design (as a single part) and enable the concatenation of multiple helices in series, the end of the helix has a D-shape (Figure 3, D). The aligning link is used to keep both waves aligned, ensure that both joints enable angular bending (Figure 3, C), and prevent relative torsional deformation between the waves. The aligning link is connected to the end of the first set of links and slides along a slotted rail in the second wave base (Figure 3,

C). The sliding does not interrupt the motion of the links in their direction of motion, but prevents the torsional rotation of the second set of links relative to the first.

C. Materials and Properties

The head and links were 3D printed using a Form2 printer with "Rigid 4000" and "Tough" materials. The links were reinforced with 0.4 mm steel pins to increase their stiffness to torsional bending and reduce the inner friction between the links and the helices. The helices, including the U-joint and the connecting links, were wax casted with brass.

III. Locomotion Analysis in a Curved Environment

This section analyzes the robot's motion in flexible environments using an energy-based approach. Given the low accelerations of the robot, we assume quasi-static locomotion in which the dynamics of motion can be neglected. The wave motion can be described as an advancing wave using:

$$y = A\sin(kx - \omega t) \quad (1).$$

where y is the height of a point located at distance x along the main axis of the wave, A is the wave's amplitude, k is the wave number, ω is the angular velocity of the helix and t is the time. Taking the second derivative with respect to time we obtain the wave's acceleration as:

$$\ddot{y} = -A\omega^2 \sin(kx - \omega t) \quad (2).$$

The maximum absolute value of the acceleration is $A\omega^2$. Given the robot's amplitude of 6.7 mm and its actuation frequency (37 RPM = 3.87 rad/s) the robot's maximal acceleration is 0.09 [m/sec^2] which can be neglected since it is two orders of magnitude lower than the acceleration of gravity, for example.

A. Energy Based Quasi-Static Analysis

Here the aim was to characterize the behavior of the robot for different friction coefficients (COF). We used an energetic approach to determine how the robot would crawl in a flexible canal as a function of the curvature of the canal, the elasticity of the walls, and the COF. Prior knowledge of the robot's tendency to rotate inside curves enabled us to design a bending joint in a specific direction which would decrease the surface energy and the robot's energy consumption. Our assumption, which was later confirmed experimentally, was that as it crawls, the robot would attempt to reduce the elastic energy of the surface by rotating its body in the roll direction. We start this section by describing the planar case of the robot advancing in a curved environment with flexible walls. For simplicity we assume that the friction forces acting on the robot at the contact points with the surface comply with the Coulomb friction model and that the kinematic and static COF are identical:

$$f_i \le \mu N_i \quad (3).$$

where μ is the friction coefficient and N_i, f_i are respectively the norms of the normal and friction forces acting on contact point i. The second assumption is that the elastic wall acts as a spring so that the normal force is linear to the deformation:

$$N_i = k \cdot \delta_i \quad (4).$$

where k is the elastic coefficient of the wall and δ_i is the radial deformation at contact point i. This assumption is based on two separate experiments conducted in our laboratory. The first experiment [29] showed that the force applied on a circular flexible tube is nearly linear (with k = 0.056 N/mm and $R^2 = 0.974$). The second experiment showed that the force to deformation in a beehive-like surface walls is also nearly linear [30] (with k = 0.155 N/mm and $R^2 = 0.949$).

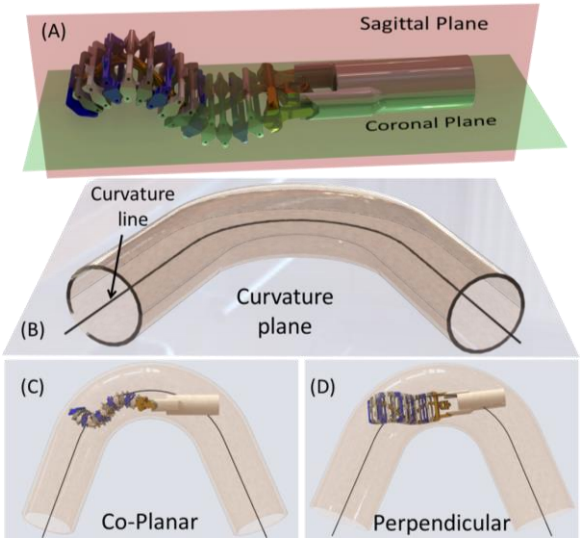

Figure 4. (A) The wave motion of the robot is contained in its sagittal plane. (B) The curvature line and plane of the tube. (C) Sagittal plane of the robot and curvature plane of the tube are co-planar. (D) Sagittal plane of the robot and curvature plane of the tube are perpendicular.

Figure 5 depicts the co-planar and perpendicular orientations while the robot is crawling inside a curved tube, where R and D are respectively the radius of the curvature and the diameter of the tube. The width of the wave is w_w, the width of the head is w_h, the length of the robot is L and the location of the center of mass (COM) is x_{cm}. The thrust force of the robot generated by the wave motion is denoted by F_{th}. As the robot enters the tube, it contacts the walls at three different points (1,2 and 3) as defined in Figure 5. We define two angles ϕ_1 and ϕ_2 which respectively relate contact points 1 and 2 to contact point 3. They can be calculated using:

$$\phi_1 = \cos^{-1}\left(\frac{R - D/2 - \delta_3 + w_w}{R + D/2 + \delta_1}\right) \quad (5).$$

and

$$\phi_2 = \cos^{-1}\left(\frac{R - D/2 - \delta_3 + (w_h + w_w)/2}{R + D/2 + \delta_2}\right) \quad (6).$$

The distance L_1 from the front tip of the robot to point 3 is calculated using:

$$L_1 = \left[\left(R + D/2 + \delta_1\right)^2 - \left(R - D/2 - \delta_3 + w_w\right)^2\right]^{1/2} \quad (7).$$

Using Eqs. (5), (6) and (7) it is now possible to calculate the sum of forces acting on the robot in the $\mathbf{e_1}$ direction:

$$N_1\left(\sin\phi_1 + \mu\cos\phi_1\right) + N_2\left(-\sin\phi_2 + \mu\cos\phi_2\right) + \mu N_3 - F_{th} = 0 \quad (8).$$

Whereas the sum of the forces in the $\mathbf{e_2}$ direction is expressed

as:

$$N_1\left(\mu\sin\phi_1-\cos\phi_1\right)+N_2\left(-\mu\sin\phi_2-\cos\phi_2\right)+N_3=0 \quad (9).$$

The sum of the torques acting on the robot relative to its COM is:

$$N_1\left[\left(x_{cm}-L\right)\left(\mu\sin\phi_1-\cos\phi_1\right)-\frac{w_w}{2}\left(\sin\phi_1+\mu\cos\phi_1\right)\right]+$$
$$N_2\left[x_{cm}\left(-\mu\sin\phi_2-\cos\phi_2\right)-\frac{w_h}{2}\left(-\sin\phi_2+\mu\cos\phi_2\right)\right]+ \quad (10).$$
$$N_3\left(x_{cm}-L_1+\frac{w_w}{2}\mu\right)=0$$

Substituting the values of the normal forces N_i, as a function of the deformations δ_i (Eq. (4)), it is possible to numerically solve the set of equations (8)-(10) and calculate the deformations δ_i and forces N_i. The total elastic energy stored in the elastic walls E_k can be calculated as a function of the deformations δ_i:

$$E_k=\sum_{i=1}^{3}\frac{k\cdot\delta_i^2}{2} \quad (11).$$

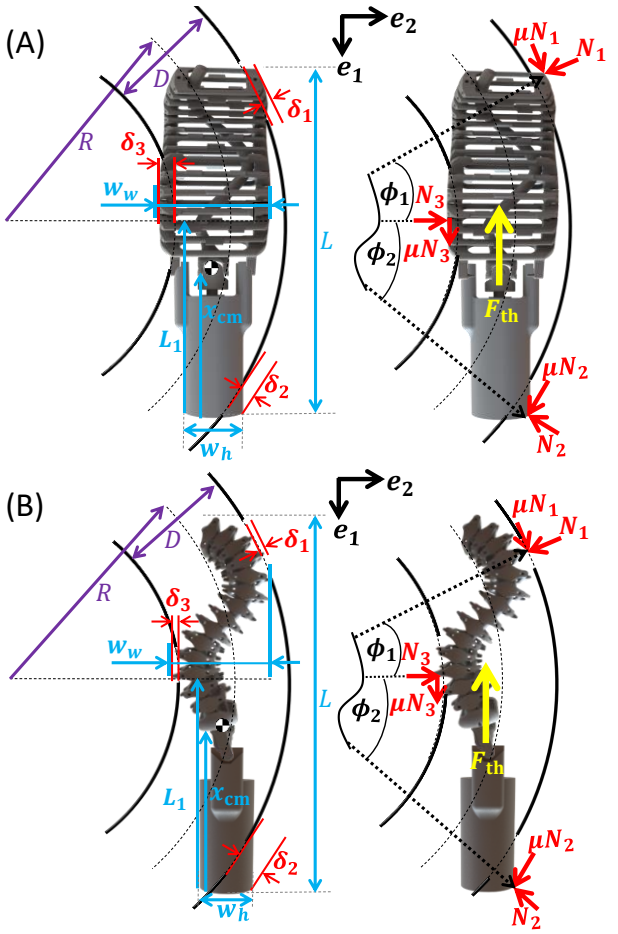

Figure 5. The forces acting on the robot and deformations of the tube as it advances. (A) Perpendicular orientation: the curvature and sagittal planes are perpendicular. (B) Co-planar orientation: the curvature and sagittal planes are co-planar.

We adjusted R and D for different COFs and two robot orientations (where the sagittal plane was perpendicular or coplanar to the curvature plane). The elastic energy as a function of R/D was calculated for different COFs in the range of [0.5, 1.1] (Figure 6).

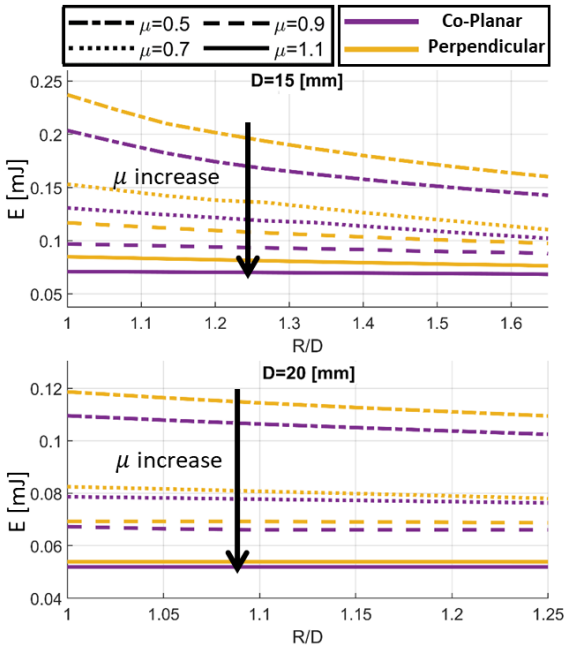

Figure 6. Elastic energy in the perpendicular and coplanar orientations for different COFs as a function of the curvature radius divided by the tube diameter. Top) The tube diameter is 15 mm. Bottom) The tube diameter is 20 mm.

The results showed that the elastic energy is larger when the width of the tube is smaller. For all COF values, the minimum energy was obtained in the coplanar configuration, where w_w was smaller; i.e., that the width/height ratio of the wave is key to determining the preferred configuration. In both configurations, the elastic energy was reduced when the COF increased. Interestingly, the relative energy difference between the two orientations became larger as the COF decreased, indicating that the coplanar configuration tended to be even more preferred when the COF was lower. In terms of both findings, it is reasonable to assume that in environments with low friction, the robot is likely to turn 90 degrees from the perpendicular to the coplanar orientation. Based on these results, we added a passive bending joint (in the sagittal plane) that would enable the robot to bend while in the coplanar orientation to reduce the robot's effective length and further decrease the elastic energy stored in the walls of the tubes.

B. Increasing the Traversability of the Robot by adding a Passive Degree of Freedom

After analyzing the preferred orientation of the robot with the energetic approach, we analyzed and quantified the difference in the threshold diameter for crawling without deformation between the former jointless version and the newer version fitted with a passive joint. We used a geometric model of the problem in which the robot has a maximum bending angle β_{max} between the head and the wave. In this model, we assume that the walls have no deformations (zero elastic energy). The boundary limits of the curvature radius R and the tube diameter D in which the robot can crawl without deforming the surface are a function of the geometric properties of the robot: L_w is the length of the wave, A is the amplitude of the wave, L_h is the length of the head, W_h is the

width of the head and β_{max} is the maximum bending angle of the head relative to the wave (Figure 7).

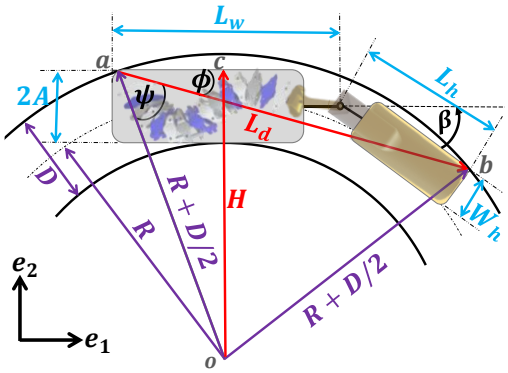

Figure 7. Robot with one bending joint crawling inside a curved pipe without deforming it.

The length of $\bar{L}_d$ is calculated using:

$$\left|\bar{L}_d\right| = \sqrt{\left(L_w + L_h\cos\beta_{max} + W_h\left(\sin\beta_{max}\right)/2\right)^2 + \left(-A - L_h\sin\beta_{max} + W_h\left(\cos\beta_{max}\right)/2\right)^2} \quad (12).$$

The angle ϕ is calculated using:

$$\phi = \tan^{-1}\left(\frac{A + L_h\sin\beta_{max} - W_h\left(\cos\beta_{max}\right)/2}{L_w + L_h\cos\beta_{max} + W_h\left(\sin\beta_{max}\right)/2}\right) \quad (13).$$

Using $\bar{L}_d$, the angle ψ can be calculated from the isosceles triangle Δoba:

$$\psi = \cos^{-1}\left(\frac{\left|\bar{L}_d\right|/2}{R + D/2}\right) \quad (14).$$

The distance H as presented in Figure 7 can be calculated using:

$$H = \left(R + D/2\right)\cdot\sin\left[\phi + \psi\right] \quad (15).$$

or alternatively using:

$$H = R - D/2 + 2A \quad (16).$$

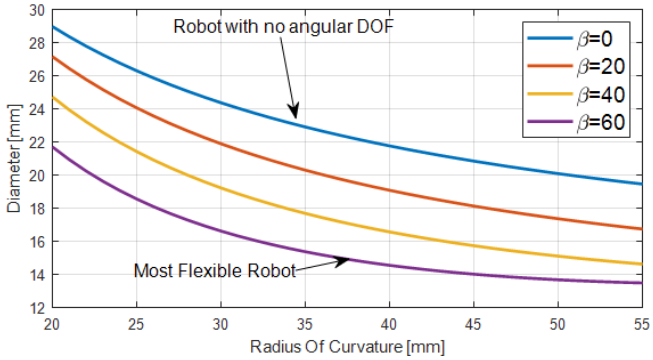

Figure 8. The tube diameter as a function of the curvature radius for different bending angles. The area above each line represents the combinations of *R,D* that allow the robot to advance freely in the tube without creating deformations. As the bending angle increases, the robot can advance in tighter environments without deforming the walls.

Equating the two equations (15) and (16) and solving numerically for different bending angles β yields the relationship between the curvature radius and the tube diameter. The threshold of D as a function of R is presented in Figure 8 for three different values of β_{max} [20, 40, 60] and compared to the case where there is no bending angle. Figure 8 shows that the added DOF with β_{max}=60° can reduce the threshold (the diameter D) by roughly 25% for the same radius R, thus allowing the robot advance in a tighter environment.

C. Crawling Expectations Based on COF

The COF of the robot's link and head to the silicone surface is 1.08. When lubricated with oil, the COF was reduced to 0.51. Figure 9 presents a surface energy comparison between the co-planar and perpendicular configurations for the two different COFs based on the deformations δ_i, calculated from equations (8)-(10) and inserted into equation (11).

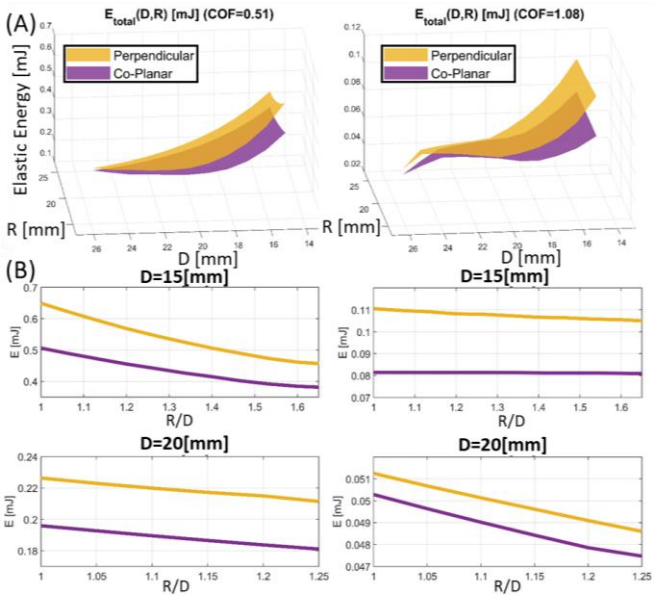

Figure 9. (A) The energy surfaces for both orientations for the measured COF (with and without lubrication). (B) Specific sections of the surface energy for D=15 mm and D= 20 mm show the preferred orientation of the robot for different diameters.

The results of the simulations, presented in Figure 6 and Figure 9, showed that the elastic energy of the surface was lower when the robot crawled in a co-planar orientation compared to the perpendicular orientation for both COFs (1.08 and 0.51). Therefore, whenever the robot starts moving in a curvature in a perpendicular orientation, it is likely to rotate its body toward the coplanar orientation.

IV. EXPERIMENTS

In this section we tested the validity of our models and the functionality of our robots using custom-built highly flexible silicon-rubber surfaces, canals and tubes. All the experimental tubes were cast using DragonSkin© silicon in 3D printed PLA molds.

A. Fabrication of Flexible Tubes and Canals

For the planar 2D experiment, we used a beehive-like structure to make the walls self-supporting (Figure 10). The beehive-like structure with a rectangular (rather than hexagonal) shape was chosen to further reduce the structural

rigidity of the silicon canal. We used square shapes rotated by 45 degrees which are easier to compress and make the structure less rigid than hexagonal shapes. The mold was composed of a canal-like shape and a cover with a large number of square rods (Figure 10, iii. and i. respectively) with very little space between them. The silicon emulsion (whose volume was equal to the gaps between the rods of the cover) was poured into the canal-like part. Then the two parts (i. and iii.) were pressed for 48 hours until the mold rigidified and then was removed.

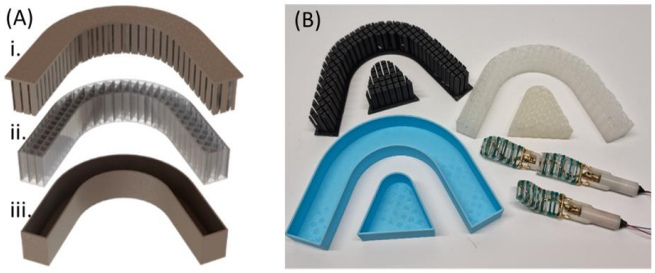

Figure 10. The fabrication procedure of the flexible tube walls using silicon rubber. (A) Silicon rubber (ii.) is poured into the two parts of the mold (i. and iii.). (B) The PLA 3D printed mold parts alongside the silicon molded walls are placed near the robots.

For the second part of our experiments, we created circular tubes using a three-part cast (Figure 11). Part ii. is enclosed between the two covers (i. and iv.) and then silicone was poured inside. Part (ii.) was supported at 4 points to (iv.) such that the gap between the tube and the outer frames remained at 1 mm. To accelerate the drying process of the silicon, vents were created in multiple locations. After solidifying, the silicon emulsion (iii.) was removed from the internal tube (ii.).

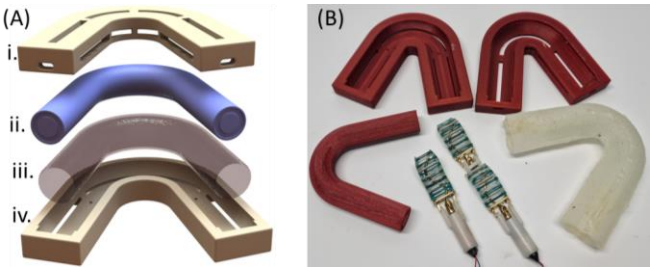

Figure 11. The fabrication process of the tubes. (A) A model of the mold and the molded tube. (B) The PLA 3D printed mold, produced silicon tube and the experimental robots.

B. Crawling between two Compliant Curved Surfaces

We tested the robot's behavior in an environment identical to the planar environment presented in the modeling section (Section III.A). We tested the previous version of the robot under two different conditions: when the silicon was lubricated (μ=0.51) and non-lubricated (μ=1.08). As expected from our energy analysis (Section III.A, Figure 9) which refers to the previous non-bending joint version, in all the runs (more than 30) the robot changed its orientation from perpendicular to co-planar for both friction cases and for different values of the turning radius R, and tube diameter D (shown in Figure 12). We repeated this experiment with our new designs (containing one and two bending joints). The same result was observed, where the robots changed their orientation from perpendicular to coplanar in all 30 runs performed on each robot.

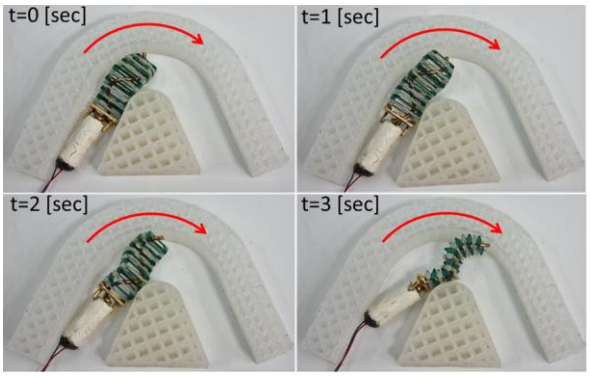

Figure 12. Snapshots of the robot advancing in the planar experimental system with $R = D = 20$ mm and $\mu = 0.51$. At $t = 0$ sec the robot is in a perpendicular orientation and rotates along its roll until completing a 90° rotation at t=3 sec.

C. Crawling inside Compliant Curved Tubes

The three versions of the robot (the simple SAW, the version with one bending joint and the version with two bending joints) were tested in tubes with a diameter of 15 mm but with a curvature radius that varied in the range R=[15,20,25,30] mm. The robots were driven in both directions, as wave leads or head leads. Each experiment was repeated 5 times and the average speed was calculated. The average speed was then normalized by the wave's speed V_w defined as the wave frequency times the wave length. The results of the experiments (summarized in TABLE I.) show that both new versions (one bending joint and two bending joints) exhibited better advancing ability than the no-joint version at different speeds.

TABLE I. THE NORMALIZED AVERAGE SPEED AND STANDARD DEVIATION OF THE ROBOTS MANEUVERING THROUGH A VARIETY OF TUBES.

Version	**crawling direction**	**Normalized speed; D=15 mm**			
		R=30 mm	R=25 mm	R=20 mm	R=15 mm
No bending joint	Wave leads	0.222 ±0.024	0.178 ±0.013	0.170 ±0.011	---
	Head leads	0.091 ±0.016	0.134 ±0.004	---	---
One bending joint	Wave leads	0.228 ±0.021	0.178 ±0.013	0.172 ±0.021	0.051 ±0.015
	Head leads	0.185 ±0.016	0.095 ±0.014	0.070 ±0.007	0.039 ±0.003
Two bending joints	Wave leads	0.137 ±0.010	0.141 ±0.004	0.150 ±0.009	0.127 ±0.005
	Head leads	0.097 ±0.007	0.088 ±0.008	---	---

The previous SAW version (with no bending joint) was able to crawl inside tubes with a curvature as low as 25 mm in both directions (wave leads and head leads) and even in 20 mm curvatures when the wave was leading. The newly designed single-joint version maneuvered successfully through all tubes in both directions at a radius of 15 mm curvature, thus demonstrating the superiority of this design in terms of traversability. The average speed of this model was equal or higher in all tubes (compared to the no-joint model); in other words, it could cover a greater distance at the same time and battery size. In terms of energy consumption, the single-joint robot also demonstrated its advantages, in that it consumed less energy than the double-joint and no-joint versions. Even in straight locomotion it reduced its energy consumption by

14% (0.103 W compared to 0.120 W) most likely because the bending joint decreased the internal friction between the links to the helix. The energy consumption in curved pipes presented in TABLE II. shows that adding the bending joints decreased the energy consumption in the curves as well.

TABLE II. THE AVERAGE POWER CONSUMED BY THE ROBOTS WHILE MANEUVERING THROUGH TUBES WITH DIFFERENT CURVATURE RADII .

Version	Average Power; D=15 mm		
	R=30 mm	R=25 mm	R=20 mm
No bending joint	0.137	0.145	0.177
One bending joint	0.111	0.120	0.120
Two bending joints	0.170	0.177	0.194

We continued testing by qualitatively comparing the deformations caused to the tubes while the robots crawled inside them. Snapshots of the initial shape of the tubes (when the robot entered it) and the maximal deformation observed in the video were taken and examined. We observed significantly fewer deformations in the tubes for the single-joint robot (Figure 13) compared to the no-joint version.

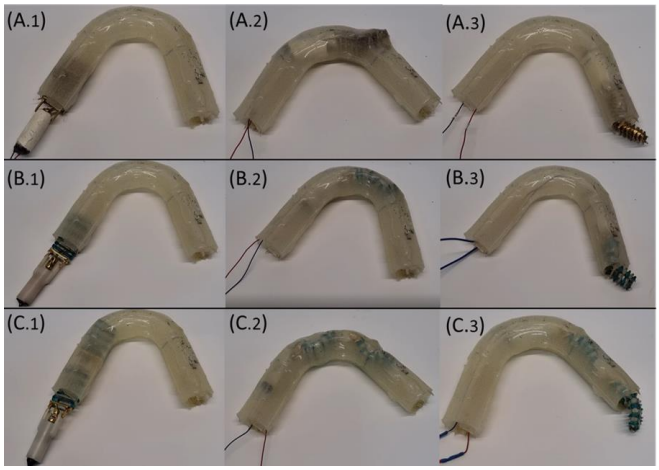

Figure 13. The robots advancing in a tube (R=25, D=15). (A1-3) No joint model. (B1-3) Single joint model. (C1-3) Double joint model.

Adding a second bending joint improved the traversability (but not the speed) compared to the no-joint version but presented no advantage over the single joint version. This robot's speed was slower than the no-joint robot, probably due to multiple contact points with the curve which increased the friction.

D. *Three Dimensional Curved Tubes*

We created a 3-dimensional curved tube that would challenge the robot to deal with multiple transitions between orientations, where the directions of the turns were perpendicular to one another. To create this experimental system, we first cast two identical U-shaped tubes and then attached them by pouring silicon rubber on the platform.

The robot successfully advanced inside the tube, rotating to change its orientation at each curve. It also climbed up the tube against gravity (Figure 14, C). Note that the previous design without a bending joint was unable to climb through the curvatures of the tube.

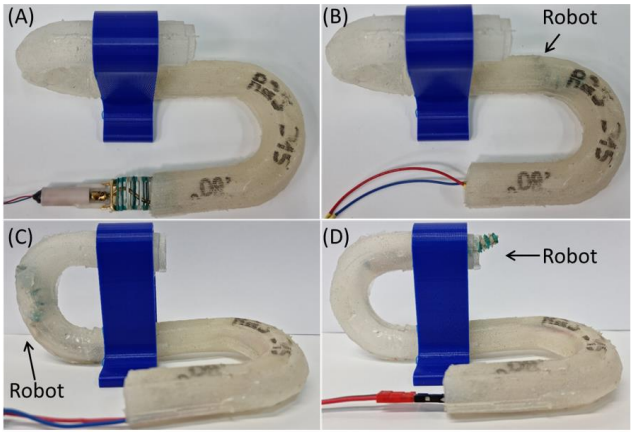

Figure 14. A 3D tube with two curves in different directions, held by a supporting beam. (A) The robot enters the tube in a perpendicular configuration, then rotates by 90º (B) as it advances through the first curve (rotating to co-planar configuration). In the next curve the robot rotates again by 90º (C) and exits the tube in (D). (See video).

E. *Vertical Climbing*

Finally, we tested all our robots in vertical straight tubes (Figure 15) to measure their advancing speed. All the designs were able to easily climb up the tube in both crawling directions, head and wave lead. The normalized average speed of the design with one bending joint was 0.316 whereas the normalized average speed of the design with two bending joints was 0.272.

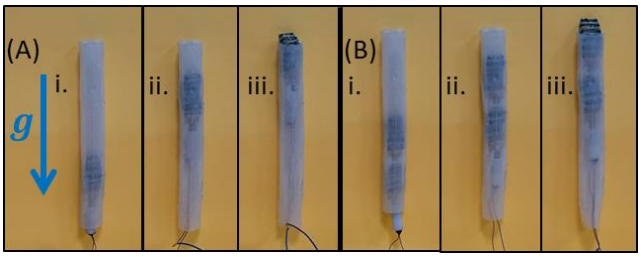

Figure 15. Robots crawling upwards against gravity. (A.i-iii) Single joint robot. (B.i-iii) Double joint robot. (see video).

V. CONCLUSION

This paper presented a locomotion analysis of a miniature wave-like robot SAW in curved compliant tubes and pipes. First, we analyzed the interaction between the robot and compliant curved surfaces and calculated the elastic energy stored in the walls while the robot advanced. The energy was calculated based on the deformation of the flexible walls using experiments we performed to determine the elasticity of the surface. Specifically, we found that the elastic energy of the tube was lower when the wave motion (sagittal plane) was coplanar to the tube curve. Given that mechanical systems aspire to reach a state of minimum energy, we expected that the robot would rotate in its roll direction along the curvatures of the tubes to minimize the elastic energy. This result was later confirmed, as in a total of more than 100 runs, the robots always rotated from a perpendicular configuration to a coplanar configuration. This led to the design of two new robotic versions with one and two passive bending joints (in the sagittal plane) to provide more flexibility along curvatures and further reduce the elastic energy of the walls.

We designed and manufactured multiple flexible tubes with different geometries to test the locomotion performance and limits of the different robotic versions and validate our results. Running the experiments revealed that the bending joints increased the robot's performance (as predicted using our energetic modeling). The single joint model exhibited improved ability to overcome acute curves. It advanced along curvatures whose radii were 25% smaller (compared to the no joint version) when the head led and 40% smaller when wave led, and also reduced the deformations of the tubes. Its energy consumption was reduced by 20-45% depending on the curvature. The robot fitted with two bending joints provided no advantages in terms of performance over the single joint, possibly because the larger number of grip points increased the internal friction between the waves and helices. However, it outperformed the previous model (with no joints) in terms of traversability and showed a smaller absolute change in energy consumption when the curvature decreased. The single joint version was also able to climb in 3D tubes with horizontal and vertical curvatures and climb vertically. These abilities to advance in different tubular flexible environments make the single-joint version the preferred SAW design.

Our future goals include making the robot more compatible with biological vessels. We plan to use more rounded shapes for the motor head and the wave of the robot to further reduce the friction with the surface. We also plan to design a wireless version integrated with a controller and battery in the robot's head, and to reduce the size of the robot even further. Specifically, while it is possible to further decrease the size of the tail (using laser cutting technology for example), the smallest rotational motors have a diameter of 2-4 mm. Further miniaturization would require finding other technologies to power the helix's motion.

VI. ACKNOWLEDGMENTS

This study was supported in part by the Israel Science Foundation, Grant No. 1279/18 and the Ministry of Science and Technology, Grant No. 3-16645.

REFERENCES

[1] G. Iddan, G. Meron, A. Glukhovsky, P. Swain, "Wireless capsule endoscopy", *Nature*, vol. 405, pp. 417-417, 2000.

[2] K.D. Wang, G.Z. Yan, "Research on measurement and modeling of the gastro intestine's frictional characteristics", *Measurement Science & Technology*, vol. 20, no. 1, 015803, 2009.

[3] Y.C. Fung, "Smooth Muscles," in "*Biomechanics: Mechanical Properties of Living Tissues*", 2nd ed., New York, 1993, pp. 466-496.

[4] X. Wang, M.Q.H. Meng, Study of frictional properties of the small intestine for design of active capsule endoscope", IEEE RAS & EMBS International Conference on Biomedical Robotics and Biomechatronics, pp. 124-129, 2006.

[5] C. Zhang, H. Liu, "Analytical friction model of the capsule robot in the small intestine", *Tribology Letters*, vol. 64, no. 3, pp. 1-11, 2016.

[6] B. Kim, M.G. Lee, Y.P. Lee, Y. Kim, G. Lee, "An earthworm-like micro robot using shape memory alloy actuator", *Sensors and Actuators, A: Physical*, vol. 125, no. 2, pp. 429-437, 2006.

[7] K. Wang, G. Yan, P. Jiang, D. Ye, "A wireless robotic endoscope for gastrointestine", *IEEE Transactions on Robotics,* vol. 24, no.1, pp. 206-210, 2008.

[8] A. Menciassi, D. Accoto, S. Gorini, P. Dario, "Development of a biomimetic miniature robotic crawler", *Autonomous Robots*, vol. 21, no.2, pp. 155-163, 2006.

[9] D. Glozman, N. Hassidov, M. Senesh, M. Shoham, "A self-propelled inflatable earthworm-like endoscope actuated by single supply line", *IEEE Transactions on Biomedical Engineering*, vol. 57, no. 6, pp. 1264-1272, 2010.

[10] K. Wang, G. Yan, G. Ma, D. Ye, "An earthworm-like robotic endoscope system for human intestine: Design, analysis, and experiment", *Annals of Biomedical Engineering,* vol. 37, no. 1, pp. 210-221, 2009.

[11] D. Zarrouk, I. Sharf, M. Shoham, "Conditions for worm-robot locomotion in a flexible environment: theory and experiments", *IEEE Transaction on Biomedical Engineering,* vol. 59, no. 4, pp. 1057-1067, 2012.

[12] D. Zarrouk, M. Shoham, "Analysis and design of one degree of freedom worm robots for locomotion on rigid and compliant terrain", *ASME, Journal of Mechanical Design*, vol. 134, no. 2, 2012.

[13] P. Dario, P. Ciarletta, A. Menciassi, B. Kim, "Modeling and experimental validation of the locomotion of endoscopic robots in the colon", *International Journal of Robotics Research*, vol. 23, no. 4-5, pp. 549-556, 2004.

[14] I. Kassim, L. Phee, W.S. Ng, F. Gong, P. Dario, C.A. Mosse, "Locomotion techniques for robotic colonoscopy", *IEEE Engineering in Medicine and Biology Magazine*, vol. 25, no. 3, pp. 49-56, 2006.

[15] V.K. Asari, S. Kumar, I.M. Kassim, "A fully autonomous microrobotic endoscopy system", *Journal of Intelligent and Robotic Systems*, vol. 28, pp. 325–341, 2000.

[16] A.B. Slatkin, J. Burdick, W. Grundfest, "The Development of a Robotic Endoscope", Experimental Robotics IV, vol. 223, pp. 162-171, 1995.

[17] S. Hirose, E.F. Fukushima, "Snakes and Strings: New Robotic Components for Rescue Operations", *International Journal of Robotics Research*, vol. 23, pp. 341-349, 2004.

[18] J. Ostrowski, J. Burdick, "kinematics for a serpentine robot", IEEE International Conference on Robotics and Automation, vol. 2, pp. 1294-1299, 1996.

[19] A. Wolf, H.H. Choset, B.H. Brown, R.W. Casciola, "Design and Control of a Mobile Hyper-Redundant Urban Search and Rescue Robot", *International Journal of Advanced Robotics,* vol. 19, no. 8, pp. 221-248, 2005.

[20] M. Mori, S. Hirose, "Locomotion of 3D Snake-Like robots – Shifting and rolling Control of Active Cord Mechanism ACM-R3", *Journal of Robotics and Mechatronics*. vol. 18, no. 5. 2006.

[21] A. Menciassi, S. Gorini, G. Pernorio, P. Dario, "A SMA actuated artificial earthworm", IEEE International Conference on Robotics and Automation, pp. 3282-3287, 2004.

[22] B. Kim, S. Lee, J.H. Park, J.O. Park, "Design and fabrication of a locomotive mechanism for capsule-type endoscopes using shape memory alloys (SMAs) ", *IEEE/ASME Transactions on Mechatronics*, vol. 10, no.1, pp. 77-86, 2005.

[23] M. Gao, C. Hu, Z. Chen, H. Zhang, S. Liu, "Design and fabrication of a magnetic propulsion system for self-propelled capsule endoscope", *IEEE Transactions on Biomedical Engineering*, vol. 57 no. 12, pp. 2891-2902, 2010.

[24] P. Valdastri, R.J. Webster, C. Quaglia, M. Quirini, A. Menciassi, P. Dario, "A new mechanism for mesoscale legged locomotion in compliant tubular environments", *IEEE Transactions on Robotics*, vol. 25 no. 5, pp. 1047-1057, 2009.

[25] A.S. Boxerbaum, K.M. Shaw, H.J. Chiel, R.D. Quinn, "Continuous wave peristaltic motion in a Robot", *The International Journal of Robotics Research*, vol. 31, no. 3, pp. 302–318, 2012.

[26] K.A. Daltorio, A.S. Boxerbaum, A.D. Horchler, K.M. Shaw, H.J. Chiel, R.D. Quinn, "Efficient worm-like locomotion: slip and control of soft-bodied peristaltic robots", *Bioinspiration and Biomimetics*. Vol. 8, 2013.

[27] D. Zarrouk, M. Mann, N. Degani, T. Yehuda, N. Jarbi, A. Hess, "Single actuator wave-like robot (SAW): Design, modeling, and experiments", *Bioinspiration and Biomimetics*, vol. 11, no. 4. 2016.

[28] D. Shachaf, O.Inbar, D. Zarrouk, "RSAW, A Highly Reconfigurable Wave Robot: Analysis, Design, and Experiments", *IEEE Robotics and Automation Letters*, vol. 4, no. 4, pp. 4475-4482, 2019.

[29] L.H. Drory, D. Zarrouk, "Locomotion dynamics of a miniature wave-like robot, modeling and experiments", IEEE International Conference on Robotics and Automation, pp. 8422-8428, 2019.

[30] N. Dgani, "Single actuator wave-like robot locomotion", M.S. thesis, Dept. Mech. Eng., Ben-Gurion University of the Negev, Israel, 2017.